LACO-OFDM with Index Modulation for Optical Wireless Systems

Ali Waqar Azim, Yannis Le Guennec, Marwa Chafii, Laurent Ros

LACO-OFDM with Index Modulation for Optical Wireless Systems

Ali Waqar Azim, Yannis Le Guennec, Marwa Chafii, and Laurent Ros

***Abstract*—In this letter, we propose layered asymmetrically clipped optical-orthogonal frequency-division multiplexing (LACO-OFDM) with index modulation (IM), i.e., LACO-OFDM-IM for optical wireless systems. In classical LACO-OFDM, the spectral leakage because of out-of-band clipping harmonics increases the baseband bandwidth (BB) resulting in lower spectral efficiencies. For LACO-OFDM-IM, we use IM and optimize the BB by filtering the out-of-band clipping harmonics. This amalgamation of IM and BB optimization leads to better spectral efficiency (SE). Simulation results shall affirm that LACO-OFDM-IM achieves higher SE, affords a comprehensive granularity for SE/energy efficiency trade-off, and outperforms classical alternatives in terms of bit-error-rate in both line-of-sight and time-dispersive channels.**

***Index Terms*—Discrete Fourier transform, orthogonal frequency-division multiplexing, index modulation, intensity-modulation and direct-detection, optical wireless systems.**

I. INTRODUCTION

INTENSITY-modulation and direct-detection based optical-orthogonal frequency-division multiplexing (O-OFDM) techniques for optical wireless systems (OWS) have been comprehensively elucidated in the literature. Among these state-of-the-art approaches, asymmetrically clipped O-OFDM (ACO-OFDM) is widely recognized for its higher energy efficiency (EE) [1]. Albeit its high EE, the spectral efficiency (SE) is low because it only uses odd complex sub-carriers (CSCs) and suffers from baseband bandwidth (BB) enlargement resulting from out-of-band clipping harmonics. To augment the SE of ACO-OFDM, layered ACO-OFDM (LACO-OFDM) is proposed [2]. LACO-OFDM populates the idle CSCs of ACO-OFDM by creating additional layers, where each succeeding layer populates the odd number CSCs left by the preceding layer. Thus, the number of CSCs reduces by a factor of two with each additional layer. This frame structure allows to increase the SE with each additional layer. Like ACO-OFDM, the negative amplitude excursions in LACO-OFDM are eliminated by clipping the asymmetric bipolar time-domain (TD) signal at each layer. However, clipping results in out-of-band clipping harmonics, thus, LACO-OFDM's BB is twice relative to real bipolar pure frequency tone based signal. This aforesaid issue of bandwidth widening is circumvented by filtered ACO-OFDM (FACO-OFDM); which filters out-of-band clipping harmonics. FACO-OFDM can reduce the BB by up to 50% relative to ACO-OFDM. It is also highlighted that a variant of LACO-OFDM which optimizes the BB does not exist in the literature. Moreover, the classical approaches, such as ACO-OFDM, FACO-OFDM and LACO-OFDM do not offer granularity for SE/EE trade-off; which is important for applications requiring varying SE and/or EE such as Internet-of-Things (IoT), and optimization of system performance based on channel conditions.

From radio-frequency (RF) literature, it is gathered that index modulation (IM) enhances the SE and imparts granularity for SE/EE trade-off [3]. Inspired by these benefits, IM adaptations for O-OFDM are elucidated in [4], [5], [6]. [4] studies an amalgam of ACO-OFDM with IM (ACO-OFDM-IM), whilst [6] investigates its enhanced variant, ACEO-OFDM-IM. Nonetheless, these IM techniques also exhibit some shortcomings: (i) their BB is not optimal; and (ii) they are only energy-efficient for low alphabet cardinalities.

The proposed LACO-OFDM-IM uses the layering configuration, optimizes the BB and integrates IM to augment the SE and to impart granularity for SE/EE trade-off. For LACO-OFDM-IM, we adopt the IM precept of [6] which involves using real virtual sub-carriers (VSCs) as it leads to higher index-domain information. Moreover, we employ Pascal's Triangle (PT) based index mapping and de-mapping to reduce the overall system complexity (see [6] for details). A layered version of OFDM-IM (for RF) is studied in [7]. However, it is not compatible with OWS as the TD signal is neither non-negative nor real. Moreover, its frame structure is entirely different from the proposed LACO-OFDM-IM. Simulation results shall reveal the following concrete advantages of LACO-OFDM-IM over state-of-the-art counterparts: (i) higher achievable SE; (ii) comprehensive granularity for SE/EE trade-off; and (iii) better EE; (iv) better bit-error-rate (BER) in line-of-sight (LOS) and time-dispersive channels.

We organize the rest of the article as follows. Section II presents the transceiver configuration. Section III compares the SE, SE/EE trade-off and the BER performance of LACO-OFDM-IM with classical counterparts and the conclusions are rendered in Section IV.

II. TRANSCEIVER CONFIGURATION OF LACO-OFDM-IM

A. Transmitter Architecture

Consider LACO-OFDM-IM transmitter with $\mathcal{L}$ layers and N CSCs. For each symbol, the equiprobable bit sequence of length λ is partitioned into $\mathcal{L}$ bit sequences each of length λ_l, where $l \in [\![1, \mathcal{L}]\!]$. λ_l is further split into λ_l^{IM} IM bits, and λ_l^{C} constellation bits. At lth layer, $N/2^{l+1}$ CSCs or equivalently $N/2^l$ real VSCs are available for IM [6]. λ_l^{IM} bits generate an integer, $Z_l \in [\![0, 2^{\lambda_l^{\mathrm{IM}}} - 1]\!]$, which identifies κ_l VSCs to be activated among the $N/2^l$ available. The indices of active sub-carriers form the sub-carrier activation pattern (SCAP) for the lth layer, $\theta_{l,k} = \{\theta_{l,1}, \theta_{l,2}, \cdots, \theta_{l,\kappa}\}$, where $k \in [\![1, \kappa_l]\!]$. By using PT based index mapping rather than combinatorial mapping, the complexity can be reduced $\mathcal{O}(2^{-l}N)$ from $\mathcal{O}(2^{-(l+1)}N^2)$. λ_l^{C} bits generate κ_l M-pulse-amplitude modulation (PAM) alphabets, $\mathcal{X}_l[k]$ which ought to be modulated on the VSCs identified via $\theta_{l,k}$. Thus, the total number of bits transmitted per LACO-OFDM-IM symbol consisting of $\mathcal{L}$ layers of duration T_{s} is

Ali Waqar Azim is with CEA Leti, MINATEC, 38054, Grenoble, France (email: aliwaqarazim@gmail.com)

Yannis Le Guennec and Laurent Ros are with Université Grenoble Alpes, CNRS, Institute of Engineering, Grenoble INP, GIPSA-LAB, 38000 Grenoble, France (email: {yannis.le-guennec,laurent.ros}@grenoble-inp.fr).

Marwa Chafii is with ETIS, UMR 8051, CY Cergy Paris Université, ENSEA, CNRS, 95000 Cergy, France (email: marwa.chafii@ensea.fr)

$$\lambda^{\mathrm{LACO-IM}} = \sum_{l=1}^{\mathcal{L}} \lambda_l = \sum_{l=1}^{\mathcal{L}} \lambda_l^{\mathrm{IM}} + \lambda_l^{\mathrm{C}}, \quad (1)$$

where the number of bits on the lth layer is

$$\lambda_l = \lambda_l^{\mathrm{IM}} + \lambda_l^{\mathrm{C}} = \left\lfloor \log_2 \binom{N/2^l}{\kappa_l} \right\rfloor + \log_2(M^{\kappa_l}), \quad (2)$$

with $\lfloor\cdot\rfloor$ and $\binom{\cdot}{\cdot}$ being the floor function and binomial coefficient, respectively.

Lemma 1. *Considering N CSCs and M-PAM, the maximum SE for LACO-OFDM-IM is attained when the number of activated VSCs per layer is approximately equal to*

$$\kappa_l^{\mathrm{approx}} \approx \left\lfloor \frac{MN}{2^l(M+1)} \right\rfloor. \quad (3)$$

Proof. Let us consider λ_l, for which, the following inequality must hold

$$\lambda_l \leq \log_2 \binom{N/2^l}{\kappa_l} + \log_2(M^{\kappa_l}). \quad (4)$$

Taking the first derivative of (4) with respect to κ_l leads to

$$\frac{\mathrm{d}\lambda_l}{\mathrm{d}\kappa_l} \leq \frac{\mathcal{H}_{N/2^l-\kappa_l} - \mathcal{H}_{\kappa_l} + \log(M)}{\log(2)}, \quad (5)$$

where $\mathcal{H}_m \approx \log(m) + \varepsilon$ is the mth harmonic number with ε being the Euler-Mascheroni constant. Substituting ${}^{\mathrm{d}\lambda_l}/_{\mathrm{d}\kappa_l} = 0$ and re-introducing the floor leads to (3). □

Lemma 1 is attained owing to the log-concavity of the binomial coefficient. It may be noticed that there may be a marginal disparity between κ_l and $\kappa_l^{\mathrm{approx}}$ because $\kappa_l^{\mathrm{approx}}$ is evaluated by ignoring the floor function. Moreover, closed-form expressions developed in [8] can be used to determine the number of VSCs resulting in maximum SE. Nonetheless, these expressions also lead to approximate values of κ_l.

Using $\mathcal{X}_l[k]$ and $\theta_{l,k}$,we attain the VSCs vector, $S_l[\zeta]$ for $\zeta \in [\![1, N/2^l]\!]$ as

$$S_l[\zeta] = \begin{cases} \sqrt{(1/2\kappa_l)}\mathcal{X}_l[k], & k \in \theta_{l,k} \\ 0, & \text{otherwise} \end{cases}, \quad (6)$$

from which, we obtain $\dot{X}_l[\gamma] = S_l[\gamma] + jS_l[\gamma + N/2^{l+1}]$, where $\gamma \in [\![1, N/2^{l+1}]\!]$ and $j^2 \triangleq -1$. For lth layer, we have $N/2^{l+1}$ elements $\dot{X}_l[\gamma]$ from the signal space [6]; which are modulated onto the $N/2^{l+1}$ CSCs of the same layer. The lth layer frequency-domain (FD) symbol, over-sampled by L comprising of N CSCs is $X_l[\sigma]$ for $\sigma \in \Omega = [\![-LN/2, LN/2 - 1]\!]$. An over-sampling factor of $L \geq 4$ is needed for the envelop characteristics of O-OFDM (IM/non-IM) to converge [9]. The FD symbol conforming to Hermitian symmetry is given as

$$X_l[\sigma] = \begin{cases} \dot{X}_l[\gamma] & \sigma = \sigma^+ \in \Omega^+ \\ \dot{X}_l^*[\gamma] & \sigma = \sigma^- \in \Omega^- \\ 0 & \text{otherwise} \end{cases}. \quad (7)$$

Let $\mu(\gamma, l) = 2^{l-1}[2(\gamma-1)+1]$, then $\sigma^+ = \mu(\gamma, l) \in \Omega^+ \in [\![0, N/2]\!]$ and $\sigma^- = -\mu(\gamma, l) \in \Omega^- = [\![-1, -N/2]\!]$. Moreover, $(\cdot)^*$ is the complex conjugate. Subsequently, using LN-order inverse fast Fourier transform (IFFT), $X_l[\sigma]$ is transformed to a real bipolar TD signal, $x_l^{\mathrm{BP}}(n)$ for $n \in [\![1, LN]\!]$, which adheres to the anti-symmetric property, i.e., $x_l^{\mathrm{BP}}(p) = -x_l^{\mathrm{BP}}(p + LN/2)$ with $p \in [\![1, LN/2]\!]$. Subsequently, $x_l^{\mathrm{BP}}(n)$ is clipped to attain real non-negative TD signal, $x_l^{\mathrm{clip}}(n) = x_l^{\mathrm{D}}(n) + x_l^{\mathrm{C}}(n)$, where $x_l^{\mathrm{D}}(n) = 0.5x_l^{\mathrm{BP}}(n)$ is the TD data carrying signal, and $x_l^{\mathrm{C}}(n) = 0.5|x_l^{\mathrm{BP}}(n)|$ is the TD clipping distortion. The out-of-band clipping, i.e., $X_l^{\mathrm{C}}\sigma] = \mathrm{IFFT}\{x_l^{\mathrm{C}}(n)\}$ cause spectral leakage, thus, the BB for $x_l^{\mathrm{clip}}(n)$ is approximately $B^{\mathrm{ext}} \approx N/T_{\mathrm{s}}$, which is twice the BB required by a real bipolar pure frequency tones based signal, i.e., $B^{\mathrm{opt}} \approx N/2T_{\mathrm{s}}$. Once the $\mathcal{L}$ layers are populated, the clipped composite TD signal for $\mathcal{L}$ layers is attained as

$$x^{\mathrm{comp}}(n) = \sum_{l=1}^{\mathcal{L}} x_l^{\mathrm{clip}}(n). \quad (8)$$

To optimize the BB, $x^{\mathrm{comp}}(n)$ is transformed to the FD counterpart, $X^{\mathrm{comp}}[\sigma]$ using LN-order FFT. $X^{\mathrm{comp}}[\sigma]$ is then passed through a low-pass filter having bandwidth $B^{\mathrm{F}} = (N + 2\alpha - 1)/T_{\mathrm{s}}$, resulting in $X^{\mathrm{F}}[\sigma] = X^{\mathrm{comp}}[\sigma] \times H^{\mathrm{F}}[\sigma]$, where α is so-called tunability factor of the low-pass filter, and $H^{\mathrm{F}}[\sigma]$ is a rectangular window low-pass filter, i.e., $H^{\mathrm{F}}[\sigma] = 1$ for $\sigma \in [\![-N/2 - \alpha, N/2 + \alpha - 1]\!]$ and zero otherwise, where $\alpha \in [\![0, (L-1)N/2]\!]$. For B^{F}, the resulting BB required for $X^{\mathrm{F}}[\sigma]$ is $B \approx (N/2 + \alpha)/T_{\mathrm{s}}$. $X^{\mathrm{F}}[\sigma]$ when converted to $x^{\mathrm{F}}(n)$ using LN-order IFFT exhibits peak regrowth in negative amplitude excursions, thus, a bias $\beta = |\min x^{\mathrm{F}}(n)|$ is added to $x^{\mathrm{F}}(n)$ resulting in $x^+(n) = x^{\mathrm{F}}(n) + \beta$. The average electrical symbol energy of $x^+(n)$ is scaled to unity, i.e., $E_{\mathrm{s}_{(\mathrm{elec})}} = \mathbb{E}\{|x^+(n)|^2\} = \sum_n |x^+(n)|^2 = 1$, where $\mathbb{E}\{\cdot\}$ evaluates the ensemble average. After digital-to-analog conversion of $x^+(n)$, an intensity waveform, $x(t) \geq 0$ is attained and is transmitted to the optical wireless channel.

Relative to classical LACO-OFDM, the proposed LACO-OFDM-IM requires an additional LN-order IFFT and LN-order FFT to filter out-of-band clipping harmonics.

B. Receiver Architecture

The received photo-detected waveform is $y(t)$, which after analog-to-digital conversion is processed by LN-order FFT to yield $Y[\sigma]$. After zero-forcing equalization, we attain

$$\hat{Y}[\sigma] = \sum_{l=1}^{\mathcal{L}} \hat{X}_l^{\mathrm{D}}[\sigma] + \hat{X}_l^{\mathrm{C}}[\sigma], \quad (9)$$

where $\hat{X}_l^{\mathrm{D}}[\sigma]$ and $\hat{X}_l^{\mathrm{C}}[\sigma]$ are the FD counterparts of $x_l^{\mathrm{D}}(n)$ and $x_l^{\mathrm{C}}(n)$, respectively. (9) implies that to correctly detect the transmit information, the clipping distortion has to be estimated and removed, such that for the lth layer, we have

$$\hat{Y}_l[\sigma] = \hat{Y}_{(l-1)}[\sigma] - \hat{X}_l^{\mathrm{C}}[\sigma]. \quad (10)$$

For $l = 1$, the clipping distortion do not fall on the data bearing CSCs, thus, $\hat{X}_1^{\mathrm{C}}[\sigma] = 0$ and $\hat{Y}_1[\sigma] = \hat{Y}_0[\sigma] = \hat{Y}[\sigma]$. For $l > 1$, the clipping distortion of $(l-1)$th layer falling on lth layer, i.e., $\hat{X}_l^{\mathrm{C}}[\sigma]$ has to be eliminated. Note that $\hat{X}_l^{\mathrm{C}}[\sigma]$ can be forthrightly estimated once the SCAP, $\hat{\theta}_{(l-1),k}$ and $\hat{\mathcal{X}}_{(l-1)}[k]$ are determined. In the sequel, we elaborate on how $\hat{\mathcal{X}}_l[k]$ and $\hat{\theta}_{l,k}$ for the lth layer can be attained.

The data bearing CSCs for the lth layer $\dot{Y}_l[\gamma] = 2\hat{Y}_l[\mu(l,\gamma)]$ are used to determine the alphabets on the VSCs as $\ddot{Y}_l[\zeta] = [\Re\{\dot{Y}_l[\gamma]\}, \Im\{\dot{Y}_l[\gamma]\}]$, where $\Re\{\cdot\}$ and $\Im\{\cdot\}$ extract the real

TABLE I: Spectral efficiencies in bits/s/Hz of the studied approaches.

Approach	Spectral Efficiency (bits/s/Hz)
LACO-OFDM-IM	$\left[\sum_{l=1}^{\mathcal{L}} \left\lfloor \log_2 \binom{N/2^l}{\kappa_l} \right\rfloor + \log_2(M^{\kappa_l})\right] (N/2+\alpha)^{-1}$
ACEO-OFDM-IM	$\left[\left\lfloor \log_2 \binom{N/2}{\dot{\kappa}} \right\rfloor + \log_2(M^{\dot{\kappa}})\right] N^{-1}$
ACO-OFDM-IM	$\left[\left\lfloor \log_2 \binom{N/4}{\tilde{\kappa}} \right\rfloor + \log_2(\tilde{M}^{\tilde{\kappa}})\right] N^{-1}$
LACO-OFDM	$\left[\sum_{l=1}^{\mathcal{L}} N/2^{l+1} \log_2(\tilde{M})\right] N^{-1}$
FACO-OFDM	$\left[(N/4) \log_2(\tilde{M})\right] (N/2+\alpha))^{-1}$
ACO-OFDM	$\left[(N/4) \log_2(\tilde{M})\right] N^{-1}$

and imaginary components of a complex number, respectively. Hereby, we use sub-optimal energy detector (ED) to determine the SCAP, $\hat{\theta}_{l,k}$. To do so, we evaluate the energies of the VSCs as $\xi_{l,\zeta} = |\hat{\tilde{Y}}_l[\zeta]|^2$. Note that the activated VSCs have higher energies relative to the inactivate ones, thus, κ_l highest energies are retained, i.e., $\xi_{l,k}$. The indices of these κ_l VSCs sorted in descending order form the SCAP, $\hat{\theta}_{l,k}$, from which, λ_l^{IM} is determined. Subsequently, the M-PAM alphabets modulated onto the activated VSCs are attained as $\hat{\mathcal{X}}_l[k] = \hat{\tilde{Y}}_l[\hat{\theta}_{l,k}]$, using which, $\hat{\lambda}_l^{\text{C}}$ are attained. $\hat{\mathcal{X}}_l[k]$ and $\hat{\theta}_{l,k}$ are then used to estimate the clipping distortion on the succeeding layer, i.e., $\hat{X}_{(l+1)}^{\text{C}}[\sigma]$. This process continues until all the $\mathcal{L}$ layers are processed.

The receiver complexity of LACO-OFDM-IM in terms of required IFFT/FFT operations is same as that of classical LACO-OFDM.

III. Performance Analysis of LACO-OFDM-IM

A. Spectral Efficiency Analysis

LACO-OFDM-IM and ACEO-OFDM-IM use M-PAM, whereas, ACO-OFDM-IM, LACO-OFDM, FACO-OFDM and ACO-OFDM employ $\tilde{M}$-quadrature-amplitude modulation (QAM). The number of active VSCs for LACO-OFDM-IM and ACEO-OFDM-IM are $\sum_l \kappa_l$ and $\dot{\kappa}$, respectively, whereas, the number of activated CSCs in ACO-OFDM-IM is $\tilde{\kappa}$. We consider N CSCs, a symbol duration of T_{s}, and $\mathcal{L}$ layers for the layered approaches. It is recalled that the BB of LACO-OFDM-IM and FACO-OFDM is B, whereas, for the remaining approaches it is B^{ext}. In the sequel, we consider $\alpha = 0$ for LACO-OFDM-IM and FACO-OFDM. Taking into account the BB and the frame structure of each approach, we calculate the spectral efficiencies, which are summarized in Table. I.

Considering $N = 32$ and $\mathcal{L} = 3$, the evolution of spectral efficiencies of the IM approaches with respect to the $\sum_l \kappa_l$, $\dot{\kappa}$ and $\tilde{\kappa}$ is presented in Fig. 1, from which, we observe that LACO-OFDM-IM is capable of attaining high spectral efficiencies using $M = 2$. Same SE trend is expected for higher M. On the contrary, all the alternatives require significantly higher modulation alphabets to attain the same SE. The SE of LACO-OFDM-IM is between the range of $[0.3125, 2.375]$ bits/s/Hz for $\sum_l \kappa_l = 17$ and $M = 2$. It is essential to highlight here that even though the lth layer has $N/2^l$ VSCs available for IM, the number of active VSCs are $\kappa_l < N/2^l$. For maximum SE, we attain that $\{\kappa_1^{\text{approx}}, \kappa_2^{\text{approx}}, \kappa_3^{\text{approx}}\} = \{10, 5, 2\}$ using (3), whereas

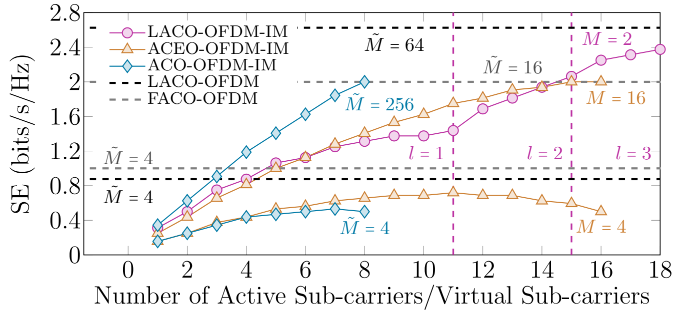

Fig. 1: (Color version online) The evolution of SE versus the κ, $\dot{\kappa}$ and $\tilde{\kappa}$ for LACO-OFDM-IM, ACEO-OFDM-IM and ACO-OFDM-IM, respectively for $N = 32$. The spectral efficiencies of LACO-OFDM and FACO-OFDM (with $\alpha = 0$) are also provided as benchmarks.

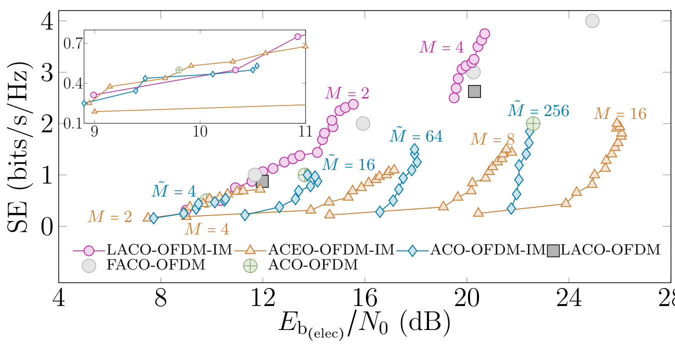

Fig. 2: (Color version online) SE/EE trade-off for LACO-OFDM-IM using $\{N, L, \alpha\} = \{32, 4, 0\}$ for BER of 10^{-3}.

the optimal values are $\{\kappa_1, \kappa_2, \kappa_3\} = \{11, 4, 2\}$. This implies that when $\kappa_l > 11$ for $l = 1$, the VSCs of $l = 2$ should be modulated and so on so forth. We observe a considerable improvement over the conventional LACO-OFDM, for which, the SE of 0.875 bits/s/Hz and 2.625 bits/s/Hz is attained using $\tilde{M} = 4$ and $\tilde{M} = 64$, respectively. This implies that LACO-OFDM requires $\tilde{M} = 64$ to attain a SE close to the maximum achievable SE of LACO-OFDM-IM. FACO-OFDM requires alphabets of lesser cardinalities relative to other approaches because of optimized BB. Moreover, for a given $\tilde{M}$, the attainable SE of ACO-OFDM (not plotted in Fig. 1) is half of SE of FACO-OFDM. Lastly, the granularity for SE/EE trade-off for IM approaches is also observable from Fig. 1.

B. Spectral-Energy Efficiency Analysis

Fig. 2 depicts the SE/EE trade-off and granularity of LACO-OFDM-IM in LOS channel. Note that for LACO-OFDM-IM, the spectral efficiencies between $[0.3125, 2.375]$ bits/s/Hz are attained using $\{M, \alpha\} = \{2, 0\}$ and $\{\kappa_1, \kappa_2, \kappa_3\} = \{11, 4, 2\}$, whilst the spectral efficiencies between the range $[2.5, 3.75]$ bits/s/Hz are achieved when $\{M, \alpha\} = \{4, 0\}$ and $\{\kappa_1, \kappa_2, \kappa_3\} = \{11, 7, 3\}$. The EE is determined by evaluating the electrical signal-to-noise ratio per bit $E_{\text{b}_{(\text{elec})}}/N_0$ required to attain a BER of 10^{-3}. $E_{\text{b}_{(\text{elec})}}/N_0$ is equal to $E_{\text{s}_{(\text{elec})}}T_{\text{s}}/(N_0\lambda^{\text{LACO-IM}})$, where N_0 is the mono-lateral noise spectral density. For a fair comparison, we use the sub-optimal ED receiver for all the IM approaches. The IM approaches generally lose their EE when alphabet cardinality increases. Interestingly, for LACO-OFDM-IM, an increase in alphabet cardinality affects the EE but it still remains the most energy-efficient approach compared to other counterparts. For example, we observe 4 dB penalty for FACO-OFDM at SE of 4 bits/s/Hz ($\tilde{M} = 256$) relative to LACO-OFDM-IM when SE is 3.75 bits/s/Hz ($\{M, \sum_l \kappa_l\} = \{4, 21\}$). Thus, from Fig. 2, we observe the following advantages of LACO-OFDM-IM over other alternatives: (i) it is the most energy-efficient and spectral-efficient approach not only for low spectral efficiencies but also for higher spectral efficiencies; and (ii) it provides the most comprehensive granularity for SE/EE trade-off for wider SE range which is impossible with classical ACO-OFDM, FACO-OFDM and LACO-OFDM. More importantly, LACO-OFDM-IM is significantly energy-efficient than its direct state-of-the-art counterpart LACO-OFDM particularly for spectral efficiencies > 1 bits/s/Hz. It is reiterated that the classical IM approaches require alphabets of higher cardinalities to attain the same peak SE as that of LACO-OFDM-IM and thus are not energy-efficient.

C. Bit-Error Rate Performance Analysis

The BER performance of LACO-OFDM-IM in LOS channel and time dispersive channel for the reference SE of 2.375 bits/s/Hz is presented in Fig. 3. In fact, this reference is the maximum achievable SE of LACO-OFDM-IM for $\{\sum_l \kappa_l, M, \alpha\} = \{17, 2, 0\}$. For ACEO-OFDM-IM and ACO-OFDM-IM, the SE close to the reference SE is 2 bits/s/Hz, which is achieved for the respective approaches for $\{M, \dot{\kappa}\} = \{16, 15\}$ and $\{\tilde{M}, \tilde{\kappa}\} = \{256, 8\}$. Moreover, we use $\mathcal{L} = 2$ and $\tilde{M} = 64$ which results in SE of 2.25 bits/s/Hz for LACO-OFDM. Lastly, $\tilde{M} = 256$ and $\{\tilde{M}, \alpha\} = \{16, 0\}$ is used for ACO-OFDM and FACO-OFDM, respectively which also result in SE of 2 bits/s/Hz. Considering data rate of 200 Mbits/s, a delay spread of 10 ns, the time-dispersive optical wireless channel is emulated using ceiling bounce model [10]. Moreover, we consider both low-complexity sub-optimal ED and maximum likelihood detector (MLD) for LACO-OFDM-IM. The MLD complexity for lth layer is $\mathcal{O}(2^l N^{-1}[2^{\lambda_l^{\mathrm{IM}}} M^{\kappa_l} + \kappa_l M])$ [6], whereas, the ED complexity is $\mathcal{O}(2^{-l} N)$. From Fig. 3, we observe that the BER performance of LACO-OFDM-IM is considerably better than classical counterparts (IM/non-IM) in both LOS and time dispersive channels with MLD exhibiting marginally better performance than ED. Note that the BER performance of ACO-OFDM-IM and ACO-OFDM is the same because all the CSCs in ACO-OFDM-IM are activated to attain 2 bits/s/Hz, thus, its frame structure is exactly the same as ACO-OFDM. It can also be observed that the BER performance of FACO-OFDM is closest to that of LACO-OFDM-IM, however, in the portrayed scenario, the SE of LACO-OFDM-IM is approximately 16% higher than the SE of FACO-OFDM. Note that for lower $E_{\mathrm{b(elec)}}/N_0$, the probability of correct detection of the active indices of VSCs is less, which, by extension also results in incorrect detection of M-PAM alphabets leading to higher BER. As $E_{\mathrm{b(elec)}}/N_0$ increases, the probability of correct detection of active indices and M-PAM alphabets improves resulting in reduction of BER. One of the reason for better BER performance of LACO-OFDM-IM is the requirement of lower alphabet cardinalities, whilst other alternatives require alphabets of significantly higher cardinality.

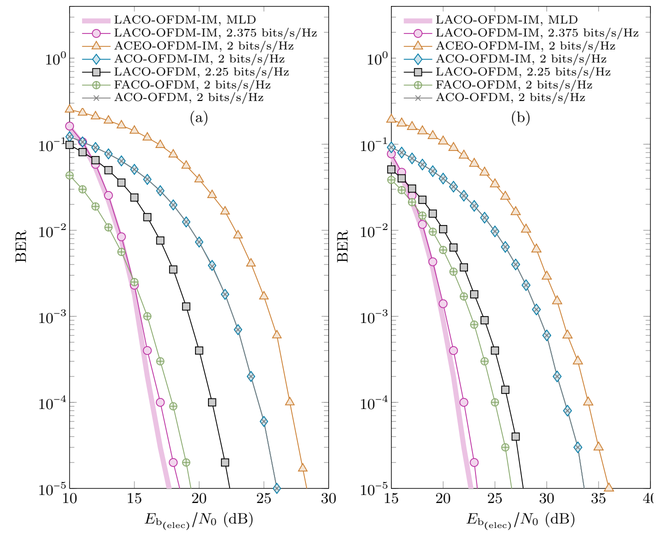

Fig. 3: (Color version online) BER performance comparison of LACO-OFDM-IM with classical counterparts for reference SE of 2.375 bits/s/Hz in (a) LOS and (b) time-dispersive channel using $N = 32$.

IV. Conclusions

In this letter, we propose LACO-OFDM-IM which employs the layering architecture, IM and BB optimization to provide significant SE gains relative to classical benchmarks. We observe that in addition to being the most energy-efficient than counterparts, LACO-OFDM-IM is capable of achieving higher spectral efficiencies and provides comprehensive granularity for SE/EE trade-off. We also analytically determine the approximate number of VSCs which maximize the SE. Moreover, the BER performance of LACO-OFDM-IM is better than classical counterparts in both LOS and time dispersive channels. These advantages of LACO-OFDM-IM portrayed herein, makes it a viable alternative to other counterparts.

References

[1] J. Armstrong and A. J. Lower. Power efficient optical OFDM. *Electron. Lett*, 42(6):370–372, 2006.

[2] Q. Wang, C. Qian, X. Guo, Z. Wang, D. G. Cunningham, and I. H. White. Layered ACO-OFDM for intensity-modulated direct-detection optical wireless transmission. *Optics Express*, 23(9):12382–12393, 2015.

[3] M. Wen, B. Zheng, K. J. Kim, M. Di Renzo, T. A. Tsiftsis, K. Chen, and N. Al-Dhahir. A survey on spatial modulation in emerging wireless systems: Research progresses and applications. *IEEE J. Sel. Areas Commun.*, 37(9):1949–1972, 2019.

[4] E. Başar and E. Panayırcı. Optical OFDM with index modulation for visible light communications. In *Intl. Wksp. Opt. Wireless Commun.*, pages 11–15, 2015.

[5] A. W. Azim, M. Chafii, Y. Le Guennec, and L. Ros. Spectral and energy efficient fast-OFDM with index modulation for optical wireless systems. *IEEE Commun. Lett.*, 24(8):1771–1774, 2020.

[6] A. W. Azim, Y. Le Guennec, M. Chafii, and L. Ros. Enhanced optical-OFDM with index and dual-mode modulation for optical wireless systems. *IEEE Access*, 8:128646–128664, 2020.

[7] J. Li, S. Dang, M. Wen, X.-Q. Jiang, Y. Peng, and H. Hai. Layered orthogonal frequency division multiplexing with index modulation. *IEEE Systems Journal*, 13(4):3793–3802, 2019.

[8] W. Li, H. Zhao, C. Zhang, L. Zhao, and R. Wang. Generalized selecting sub-carrier modulation scheme in ofdm system. In *IEEE ICC*, pages 907–911, 2014.

[9] S. Mazahir, A. Chaaban, H. Elgala, and M.-S. Alouini. Achievable rates of multi-carrier modulation schemes for bandlimited IM/DD systems. *IEEE Trans. Wireless Commun.*, 18(3):1957–1973, 2019.

[10] J. B. Carruthers and J. M. Kahn. Modeling of nondirected wireless infrared channels. *IEEE Trans. Commun.*, 45(10):1260–1268, 1997.